

Discovering an Active Subspace in a Single-Diode Solar Cell Model

Paul G. Constantine* and Brian Zaharatos
Department of Applied Mathematics and Statistics
Colorado School of Mines
and
Mark Campanelli
National Renewable Energy Laboratory

September 16, 2018

Abstract

Predictions from science and engineering models depend on the values of the model's input parameters. As the number of parameters increases, algorithmic parameter studies like optimization or uncertainty quantification require many more model evaluations. One way to combat this curse of dimensionality is to seek an alternative parameterization with fewer variables that produces comparable predictions. The *active subspace* is a low-dimensional linear subspace of the space of model inputs that captures the variability in the model's predictions. We describe a method for checking if a model admits an exploitable active subspace, and we apply this method to a single-diode solar cell model. We find that the maximum power of the solar cell has a dominant one-dimensional active subspace in its space of five input parameters.

Keywords: single diode solar cell, active subspaces

*The authors gratefully acknowledge the support Department of Energy's Advanced Scientific Computing Research Award *Mathematical and Statistical Methodologies for DOE Data-Centric Science at Scale*.

1 Introduction

Science and engineering simulations often contain several input parameters—e.g., physical constants, boundary conditions, or geometry descriptions. When presented with such parameterized simulations, the scientist naturally wonders how the simulated predictions depend on the input parameters. Which parameters, when perturbed, create the largest change in predictions? How precisely must the parameters be specified to ensure accurate predictions? And what is the effect of imprecisely prescribed input parameters on the predictions? If the goal is to maximize or minimize a predicted quantity, which combinations of parameters correspond to larger or smaller values of the prediction? In a similar vein, one may ask which parameter values correspond to predictions outside a safe region of operation—or which parameter values yield predictions that are consistent with a set of observations.

Many scientists rely on intuition about the physical system to answer these questions. But intuition becomes less trustworthy as the simulations become more complex, e.g., when they include several interacting physical components. Algorithms for optimization, uncertainty quantification, and model calibration become more attractive as model complexity increases. If an algorithm can easily interface with the simulation—e.g., by automatically evaluating predictions given values for the inputs—then applying the algorithm to the simulation becomes relatively easy.

The number of times the algorithm needs to evaluate a prediction will increase—sometimes extremely rapidly—as the number of inputs increases. The situation is worse if each evaluation requires significant computational resources. For example, finding the global minimum of a complicated prediction depending on one hundred inputs is not tractable if available resources permit only ten model evaluations. In practice, the scientist may choose only the most important parameters to vary so the study fits within the computational budget. Alternatively, one may seek a low-dimensional description of the prediction as a function of the input parameters. If such a description is sufficiently accurate, then studies like optimization or calibration can work in the space of fewer variables—potentially allowing the desired parameter studies within the given budget.

The *active subspace* is low-dimensional linear subspace of the space of input parameters

that describes the majority of variability in the model predictions. Not all models have an active subspace. Some model’s predictions vary significantly along all directions in the space of model inputs. However, if a model does admit an active subspace, then one can exploit it to perform parameter studies on the coordinates of the subspace—i.e., the *active variables*—which are linear combinations of normalized versions of the model’s input parameters. Therefore, it can be very advantageous to discover that a model admits an active subspace.

Active subspaces have been studied in a variety of contexts under different names. Cook’s excellent text *Regression Graphics* [3] reviews and develops statistical methods for dimension reduction in the context of regression surfaces, and it contains references to the major works in the statistics literature. What we call the *active subspace* is a type of *dimension-reduction subspace* in Cook’s parlance [3, Chapter 6]—though we are working with noiseless computer simulations in contrast to general regression surfaces. Russi’s 2010 Ph.D. dissertation [10] uses the phrase *active subspace* in a way comparable to our use. He exploits the active subspace to construct quadratic surrogate models for uncertainty quantification in chemical kinetics models. Our prior work [2] develops a theoretical framework for active subspaces including applications to kriging response surfaces; we have applied these methods to several models in aerospace engineering [1, 9, 13].

In this paper, we describe how to test a model for an active subspace, and we apply this test to a single-diode model of a photovoltaic solar cell with five input parameters. In the Section 2, we generically describe the active subspace and how to search for it. We then describe the single-diode model, its input parameters, and its predicted *performance parameters* (i.e., model outputs) in Section 3. We apply the tests for the active subspace to the single-diode model in Section 4 and show that a dominant one-dimensional active subspace is present in the five-dimensional space of input parameters. We conclude in Section 5 with a discussion of how one may exploit the low dimension of the active subspace to further study the parameter dependence in the single-diode model.

2 Active subspaces

We consider a generic multivariate function $f = f(\mathbf{x})$, where \mathbf{x} represents the inputs of the model, and f represents a specific scalar performance parameter that the model predicts. Let $\mathcal{X} = [-1, 1]^m$ be the normalized domain with $\mathbf{x} \in \mathcal{X}$, and let $\rho : \mathcal{X} \rightarrow \mathbb{R}_+$ be a measure on \mathcal{X} . For simplicity, we let ρ be constant on \mathcal{X} such that it integrates to one; such assumptions are common in engineering models, though this can be relaxed. Assume f is differentiable and absolutely continuous, and denote the gradient $\nabla_{\mathbf{x}}f(\mathbf{x}) = [\partial f/\partial x_1, \dots, \partial f/\partial x_m]^T$ oriented as a column vector.

We are interested in the following matrix, denoted \mathbf{C} and defined as

$$\mathbf{C} = \int_{\mathcal{X}} (\nabla_{\mathbf{x}}f)(\nabla_{\mathbf{x}}f)^T \rho d\mathbf{x}. \quad (1)$$

In the context of dimension reduction for regression functions, this matrix is called an *average derivative functional* [12]. Note that we are not studying regression functions, per se, but computer simulations symbolized by f . The matrix \mathbf{C} is symmetric and positive semi-definite, so it admits a real eigenvalue decomposition

$$\mathbf{C} = \mathbf{W}\Lambda\mathbf{W}^T, \quad \Lambda = \text{diag}(\lambda_1, \dots, \lambda_m), \quad \lambda_1 \geq \dots \geq \lambda_m \geq 0. \quad (2)$$

We can partition the eigenvectors,

$$\mathbf{W} = \begin{bmatrix} \mathbf{W}_1 & \mathbf{W}_2 \end{bmatrix}, \quad \Lambda = \begin{bmatrix} \Lambda_1 & \\ & \Lambda_2 \end{bmatrix}, \quad (3)$$

where \mathbf{W}_1 contains the first n eigenvectors, and Λ_1 contains the n largest eigenvalues. We use the two sets of eigenvectors to create new sets of variables $\mathbf{y} = \mathbf{W}_1^T\mathbf{x}$ and $\mathbf{z} = \mathbf{W}_2^T\mathbf{x}$. We call the subspace defined by \mathbf{W}_1 the *active subspace*, and we call the variables \mathbf{y} the *active variables*; the term *active subspace methods* for this type of analysis was first used in Russi's 2010 Ph.D. dissertation [10]. The following two lemmas justify these labels.

Lemma 2.1 *The mean-squared directional derivative of f with respect to the eigenvector \mathbf{w}_i is equal to the corresponding eigenvalue,*

$$\int_{\mathcal{X}} ((\nabla_{\mathbf{x}}f)^T \mathbf{w}_i)^2 \rho d\mathbf{x} = \lambda_i. \quad (4)$$

Lemma 2.2 *The mean-squared gradients of f with respect to the coordinates \mathbf{y} and \mathbf{z} satisfy*

$$\begin{aligned} \int_{\mathcal{X}} (\nabla_{\mathbf{y}} f)^T (\nabla_{\mathbf{y}} f) \rho d\mathbf{x} &= \lambda_1 + \cdots + \lambda_n, \\ \int_{\mathcal{X}} (\nabla_{\mathbf{z}} f)^T (\nabla_{\mathbf{z}} f) \rho d\mathbf{x} &= \lambda_{n+1} + \cdots + \lambda_m. \end{aligned} \tag{5}$$

The proofs of these lemmas can be found in our prior work [2]. In words, they mean that f varies more on average along the directions \mathbf{W}_1 than along the directions \mathbf{W}_2 ; the eigenvalues quantify precisely how much more. If an eigenvalue is exactly zero, then $f(\mathbf{x})$ is constant along the direction defined by the corresponding eigenvector over all of \mathcal{X} .

To gain some intuition, consider the extreme case where all eigenvalues are precisely zero except λ_1 . Then $f(\mathbf{x}) = g(\mathbf{w}_1^T \mathbf{x})$, where \mathbf{w}_1 is the first column of \mathbf{W} , and g is a univariate function. In many applications, the smaller eigenvalues are not precisely zero, but they may be much (e.g., orders of magnitude) smaller so that $f(\mathbf{x})$ may be reasonably approximated by a function of $n < m$ linear combinations of \mathbf{x} .

If a given model f admits such structure, then certain operations—e.g., response surface modeling or optimization—become much less expensive. In particular, these operations can be performed in the n -dimensional space of the active variables \mathbf{y} instead of the full m -dimensional space. It is therefore extremely valuable to determine if f admits an active subspace. Note that this analysis assumes that the measure ρ on the domain \mathcal{X} is given, and the computed quantities (like \mathbf{W} and Λ) will change if a different ρ is given.

2.1 Identifying an active subspace

To identify the active subspace, we must approximate the matrix \mathbf{C} from (1). Since \mathbf{C} is the mean of the outer product of the gradient, we can approximate it with simple Monte

Carlo¹. Draw \mathbf{x}_i independently from ρ with $i = 1, \dots, M$. Then

$$\mathbf{C} \approx \hat{\mathbf{C}} = \frac{1}{M} \sum_{i=1}^M \nabla_{\mathbf{x}} f(\mathbf{x}_i) \nabla_{\mathbf{x}} f(\mathbf{x}_i)^T = \hat{\mathbf{W}} \hat{\Lambda} \hat{\mathbf{W}}^T. \quad (6)$$

We use the eigenvalues of the approximation $\hat{\mathbf{C}}$ as evidence of the presence of an active subspace. In particular, a large gap in the eigenvalues indicates a separation between the corresponding active and inactive subspaces defined by $\hat{\mathbf{W}}_1$ and $\hat{\mathbf{W}}_2$, respectively. The qualification *large* depends on the application. For example, a good low-dimensional approximation of f over its entire domain may need a much larger separation than a good approximation of the bounds or the average of f . Other eigenvalue-based dimension reduction schemes—e.g., principal component analysis—use heuristics like choosing the dimension of the subspace such that the ratio $\sum_{i=1}^n \lambda_i / \sum_{i=1}^m \lambda_i$ is larger than some threshold. For active subspaces, such heuristics are not well justified.

If a gap is present in the approximate eigenvalues $\hat{\Lambda}$, one may naturally ask if a comparable gap is present in the true eigenvalues Λ . To address this question, we can again use simple Monte Carlo, since $\hat{\Lambda}$ is a random variable by virtue of the random samples \mathbf{x}_i used to compute it. In particular, we can repeat the process in (6) M' times to get bootstrap confidence intervals on the eigenvalues. A gap between confidence intervals provides confidence in a gap in the eigenvalues Λ . Our current research efforts are focused on quantitative metrics for determining the relationship between the approximate eigenvalues $\hat{\Lambda}$ and the true eigenvalues Λ .

2.2 Visualization with the active subspace

Scatter plots are a common way to visualize data sets in search of a trend. Unfortunately, visualization tools can only display scalar responses f as a function of at most two variables. When the response depends on more than two variables, one can plot responses versus each variable or each pair of variables.

¹One could achieve a more accurate approximation of \mathbf{C} and its eigendecomposition with an integration rule that is more accurate than simple Monte Carlo. However, if m is greater than two or three, then tensor product constructions of accurate univariate numerical integration rules (e.g., Gaussian quadrature) require too many evaluations of the gradient to be practical—especially if the gradient is expensive to compute.

Using the vectors defining the active subspace, we can create scatter plots based on the active variables, which often show discernible trends that can be exploited in further studies (e.g., building regression models or optimization). This idea is described in detail in the texts on *regression graphics* [3]. For example, suppose we have noticed a large gap between the first and second eigenvalue. We can confirm the presence of the active subspace by first sampling \mathbf{x}_i from ρ as in (6), computing $f_i = f(\mathbf{x}_i)$ (often computed along with the gradients in (6)), and plotting the pairs $(\mathbf{w}_1^T \mathbf{x}_i, f_i)$ —where \mathbf{w}_1 is the first column of \mathbf{W} . If a tight, univariate trend is visibly present, then this verifies the active subspace. Figures 2 and 3 in Section 4 show these scatter plots for the single-diode model.

These scatter plots can also be used to examine the variability in the vectors defining the active subspace. If we use simple Monte Carlo and repeat the process in (6) M' times, then we get M' samples of the vectors $\hat{\mathbf{W}}$. The first eigenvector from each can be used to create pairs for the scatter plot. Plotting all pairs together creates clusters in the scatter plot that can indicate the variation in the computed eigenvectors. We create these visualizations for the predicted performance parameter from the single-diode model in Section 4.

2.3 Gradient approximation

Often the gradient $\nabla_{\mathbf{x}} f$ is not available or is too complicated to compute. To approximate partial derivatives, one builds a model of $f(\mathbf{x})$ that is easily differentiable, e.g., a polynomial model. A finite difference approximation of the partial derivative with respect to x_i at \mathbf{x} computes the slope of the plane that interpolates f at \mathbf{x} and $\mathbf{x} + \varepsilon \mathbf{e}_i$, where \mathbf{e}_i is a vector of zeros with a one in the i th component.

If the simulation output is well behaved as a function of the variables \mathbf{x} , then finite difference approximations of gradients can be used as a substitute for the true gradient. Each finite difference approximation requires $m + 1$ evaluations of f , so the number of evaluations to compute $\hat{\mathbf{C}}$ is $M(m + 1)$. To repeat this computation M' times to study the variability in $\hat{\Lambda}$ and $\hat{\mathbf{W}}$ requires $M'(M)(m + 1)$ evaluations of f . Therefore, finite differences are most appropriate when the following are satisfied:

- the simulation output behaves well as a function of the parameters, i.e., there is no noise due to limited iterations of a nonlinear solver or large changes of the function

on scales smaller than the finite difference step size,

- the simulation completes in a short enough time on available computing resources to permit $M'(M)(m + 1)$ evaluations.

Both of these conditions are satisfied for the performance parameter of interest from the single-diode model as a function of its input parameters. Therefore, we use finite differences in place of the true gradient to search for an active subspace.

3 A single diode solar cell model

In this section we introduce the single diode solar cell model, its input parameters, and the predicted quantity of interest. Over the past decade, a growing demand for clean energy has caused rapid growth in the photovoltaic (PV) industry. The overall health of the industry depends proper characterization of the risks associated with a PV system. One can characterize such risks using a mathematical model to describe the performance of the PV device, such as a single-diode lumped-parameter equivalent-circuit model defined in Section 3.1. For many series-wired PV devices, the single-diode model accurately describes the device’s current-voltage (I - V) characteristics at given irradiance and temperature conditions; it contains several model parameters: the short-circuit current, I_{SC} (I when $V = 0$), the reverse saturation current I_S , the ideality factor, n , and the series and parallel resistances, R_S and R_P respectively. In general, these parameters may depend on irradiance, temperature, or voltage. Once the model parameters are estimated (e.g., by using methods in [6] or [5]), practitioners can estimate certain functions of the model parameters—the *key performance parameters*—such as the maximum power output, P_{max} , and energy conversion efficiency η , which are functions of irradiance and temperature. Estimating the model and performance parameters often presents challenges. For example, many single-diode model parameter estimation methods have been proposed in the PV literature, and it is not always clear if any particular estimation yields a unique result [7]. Further, since each key performance parameter is the output of a function of the model parameters; errors in estimating the latter will cause issues in estimating the former.

Given these issues, it is desirable to know how the variability or uncertainty in each of the

model parameters (inputs) affects variability in estimates of the key performance parameter (outputs). In particular, it would be useful to know whether the space of inputs admits an active subspace. If an active subspace is present, then estimation of the performance parameters is greatly simplified. For example, rather than conducting I - V measurements in a way that yields accurate estimates of all model parameters, practitioners could instead focus on measurements that accurately estimate parameters in the active subspace.

3.1 Calculating the key performance parameters

To check for an active subspace, we first define the functions that yield the key performance parameters and comment on the implementation of these functions in MATLAB. At any particular (I, V) point, the power of a PV device is defined as $P(I, V) = IV$, and the maximum power is defined as

$$P_{\max} = \max_{I, V} P(I, V). \quad (7)$$

I - V curves are measured with a discrete set of (I, V) points. Simply calculating $P(I, V)$ for each measured (I, V) pair and choosing the largest value will not necessarily yield the true P_{\max} ; the maximum power point may occur at an (I, V) point that was not measured. For this reason, we use a performance model to calculate the entire I - V curve. Then, using the entire I - V curve, we can perform the maximization over the entire (I, V) space. In this work, we use the single-diode model as a performance model²:

$$I = I_L - I_S \left(e^{\frac{V + IR_S}{N_S n V_{th}}} - 1 \right) - \frac{V + IR_S}{R_P}, \quad (8)$$

where the thermal voltage is $V_{th} := k_B T/q$, I_L is defined as

$$I_L := E I_{SC_0} + I_{S_0} \left(e^{\frac{E I_{SC_0} R_{S_0}}{N_S n_0 V_{th_0}}} - 1 \right) + \frac{E I_{SC_0} R_{S_0}}{R_{P_0}}, \quad (9)$$

and

²The single-diode model often has accompanying auxiliary equations that describe the way in which each of the parameters changes under different irradiance and temperature conditions. In this work, we use the auxiliary equations described in [14]. See [4] for an example of others.

| | |
|---|--|
| E effective irradiance (unit-less) | R_S series resistance of device (Ω) |
| I_L photocurrent (A) | R_P parallel (shunt) resistance (Ω) |
| I_S diode reverse saturation current (A) | k_B Boltzmann constant |
| N_S number of cells connected in series (unit-less) | T junction temperature (K) |
| n ideality factor of device (unit-less) | q electron charge ($1.602176487 \times 10^{19}$ C). |

The *naught* notation denotes the model parameters at standard reporting conditions (SRC) of $T = 25^\circ\text{C}$ and an irradiance of 1000 W/m^2 . For notational ease, we denote the model parameters using the vector $\boldsymbol{\theta} = (I_{SC_0}, I_{S_0}, n, R_{S_0}, R_{P_0})$. The domain of possible values for $\boldsymbol{\theta}$ is shown in Table 1. These domains include values that are typical of a 2cm^2 silicon PV cell.

Table 1: The ranges of the components of $\boldsymbol{\theta}$, which are inputs for the function yielding P_{\max} .

| Parameter | Upper bound | Lower bound | Units |
|---------------------|-------------|-------------|-----------|
| $\theta_1 = I_{SC}$ | 0.05989 | 0.23958 | amps |
| $\theta_2 = I_S$ | 2.2e-11 | 2.2e-7 | amps |
| $\theta_3 = n$ | 1 | 2 | unit-less |
| $\theta_4 = R_S$ | 0.16625 | 0.66500 | ohms |
| $\theta_5 = R_P$ | 93.75 | 375.00 | ohms |

We obtain power as a function of the data I , V , E , and fixed parameters $\boldsymbol{\theta}$ by first using Lambert W functions to solve equations (8)–(9) for I as a function of V , E , and $\boldsymbol{\theta}$, denoted $I = g_I(V, E; \boldsymbol{\theta})$ [8]. Then we multiply this function by V to obtain

$$P(V, E; \boldsymbol{\theta}) = V I = V g_I(V, E; \boldsymbol{\theta}). \quad (10)$$

For a fixed $\boldsymbol{\theta}$ and $E = 1$ (which corresponds to the irradiance value at SRC), maximizing equation (7) over the space of all values of I and V is equivalent to maximizing equation

(10) over the space of all values of V . Once the power is calculated, efficiency η is expressed as

$$\eta = \frac{P_{\max}}{AE}, \quad (11)$$

where A is the surface area of the PV cell and E is the input irradiance. Implementations of equations (10) and (11) in MATLAB constitute the model being analyzed for active subspaces in Section 4. Requests for the MATLAB code may be sent to the third author, Campanelli.

4 An active subspace in the single diode model

We apply the techniques from Section 2 to search for an active subspace of the P_{\max} performance parameter as a function of the variables $\boldsymbol{\theta}$ defined in Table 1. The MATLAB scripts for generating these figures can be found at <https://bitbucket.org/paulcon/active-subspaces-in-a->

We first normalize the domain of $P_{\max} = P_{\max}(\boldsymbol{\theta})$ to the hypercube; denote the normalized variables by $\mathbf{x} = [x_1, x_2, x_3, x_4, x_5]^T$. The variable θ_2 varies over several orders of magnitude, and preliminary tests show that P_{\max} changes rapidly near smaller values of θ_2 . To address this, we prefer to work with $\log(\theta_2)$. The range of $\log(\theta_2)$ is bounded below by -24.54 and above by -15.32. Let $\theta_{l,i}$ and $\theta_{u,i}$ be lower and upper bounds, respectively, on variable θ_i . We define the normalized variables as

$$\begin{aligned} x_i &= 2 \left(\frac{\theta_i - \theta_{l,i}}{\theta_{u,i} - \theta_{l,i}} \right) - 1, \quad i = 1, 3, 4, 5 \\ x_2 &= 2 \left(\frac{\log(\theta_2) - \log(\theta_{l,2})}{\log(\theta_{u,2}) - \log(\theta_{l,2})} \right) - 1. \end{aligned} \quad (12)$$

Then $\mathbf{x} \in [-1, 1]^5$, and we let the measure ρ be equal to 2^{-5} inside the hypercube and zero outside.

We choose $M = 50$ points \mathbf{x}_i uniformly at random from $[-1, 1]^5$, and for each \mathbf{x}_i we compute both P_{\max} and a finite difference approximation of the gradient; each sample \mathbf{x}_i from the normalized domain must be shifted and scaled (and transformed by the exponential in the second component) to the original domain to make sense with the single-diode model. We use a finite difference step size of 10^{-4} in the normalized domain.

To study variability in the computed components of $\hat{\mathbf{C}}$ from (6), we repeat the procedure $M' = 200$ times. The bootstrap 95% confidence intervals for the eigenvalue estimates are shown in Table 2. There is a gap of nearly an order of magnitude between both the first and second and the second and third eigenvalues. This suggests a very dominant one-dimensional active subspace.

Table 2: The bootstrap 95% confidence bounds on the eigenvalues of $\hat{\mathbf{C}}$ sampled $M' = 200$ times. The order-of-magnitude gaps between the ranges provide confidence in the dominance of the active subspace.

| Eigenvalue | Lower 95% confidence limit | Upper 95% confidence limit |
|-------------------|----------------------------|----------------------------|
| $\hat{\lambda}_1$ | 2.9107e-03 | 3.7868e-03 |
| $\hat{\lambda}_2$ | 1.0757e-04 | 2.1902e-04 |
| $\hat{\lambda}_3$ | 1.2352e-05 | 3.0340e-05 |
| $\hat{\lambda}_4$ | 4.4046e-07 | 3.1215e-06 |
| $\hat{\lambda}_5$ | 2.0545e-07 | 5.3533e-07 |

Figure 1 displays the 200 realizations of the components of the first and second eigenvectors from the estimates $\hat{\mathbf{C}}$ —along with the components computed with all 10000 samples of the gradients. They are normalized so that the first component is positive. The small ranges suggest that the one- and two-dimensional active subspaces are stable.

These components connect the active subspace to the (normalized) variables in the model; Figure 1 includes the corresponding labels in the x -axis. The magnitudes of the eigenvector components can be used as measures of relative sensitivity for each of the parameters in the model. A large absolute value of the eigenvector component implies that this variable is important in defining the direction that produces the most change (on average) in the model output. The component corresponding the parallel resistance R_P is close zero, which implies that changes in R_P do not cause as much change to P_{\max} as the other parameters. A sensitivity analysis that was limited to model variables (e.g., variance-based decompositions that use Sobol indices [11]) would likely conclude that four of the five coordinate dimensions were important. However, the rotation of the domain

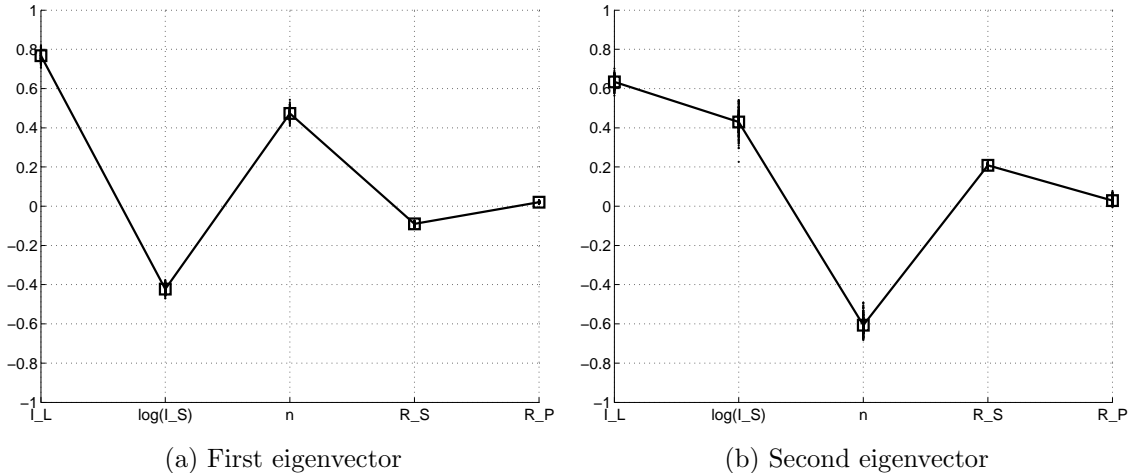


Figure 1: These figures show the components of the first (left) and second (right) eigenvectors of $\hat{\mathbf{C}}$ over $M' = 200$ independent realizations. The squares are the components of the eigenvectors of $\hat{\mathbf{C}}$ using all 10000 realizations of the gradient. The narrow ranges of values indicate that the computed subspaces are stable. These values can be used as measures of sensitivity of P_{\max} with respect to the input variables in the model, whose names are given along the x -axis of the figures. See Table 1 for a description of the variables.

produced by the eigenvector matrix \mathbf{W} allows for a much more general sensitivity analysis.

Figure 2a plots 20 values of P_{\max} with input variables projected with the one-dimensional active subspaces from the Monte Carlo estimates of the first eigenvector $\hat{\mathbf{w}}_1$. The horizontally oriented clusters contain projections using all 200 samples of $\hat{\mathbf{w}}_1$; the black squares are the projection using $\hat{\mathbf{w}}_1$ computed with all $(M)(M') = 10000$ realizations of the gradient. The clusters show the effect of finite sampling on the projections along \mathbf{w}_1 . A strong univariate trend is present in the samples of P_{\max} when viewed from the angles defined by the eigenvector \mathbf{w}_1 , which further verifies the dominance of the one-dimensional active subspace.

Figure 2b is a scatter plot, with grayscale corresponding to the vertical component, of the same 20 values of P_{\max} and the variation due to the eigenvectors $\hat{\mathbf{w}}_1$ and $\hat{\mathbf{w}}_2$. Each shaded cluster corresponds to one value of P_{\max} ; the back dots are the projections using $\hat{\mathbf{w}}_1$ and $\hat{\mathbf{w}}_2$ computed with all $(M)(M') = 10000$ realizations of the gradient. The dominance

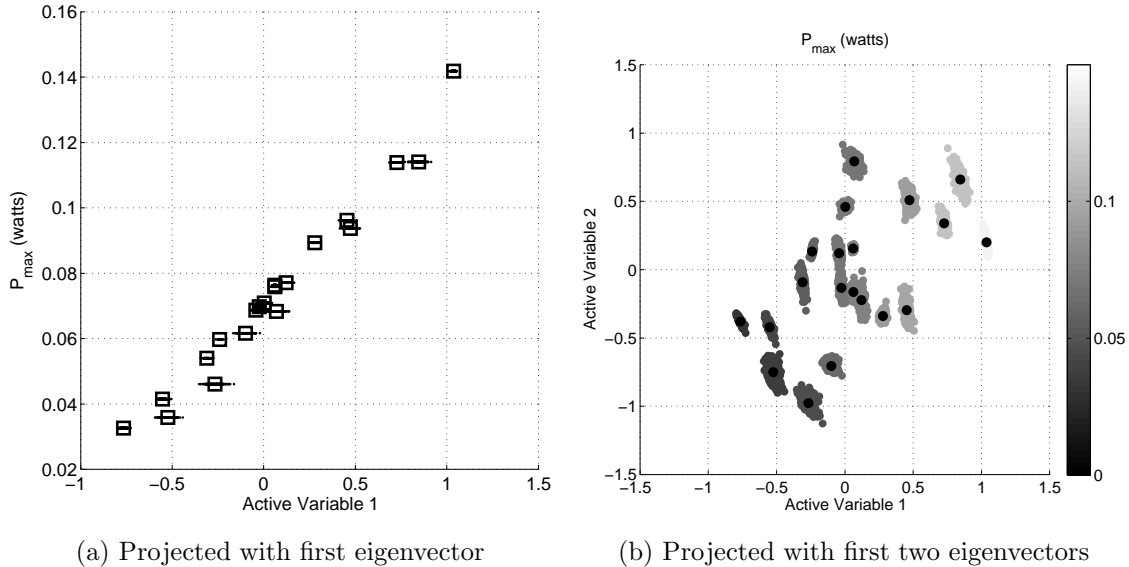


Figure 2: Visualizations of 20 selected realizations of P_{\max} with the inputs projected using the one-dimensional and two-dimensional active subspaces. The clusters of points correspond to variation in the Monte Carlo samples of the eigenvectors of $\hat{\mathbf{C}}$. The strong trend in 2a is verified by looking at the variation along *Active Variable 1* (the x -axis) in 2b, and the combination of these provide evidence of a dominant active subspace.

of the one-dimensional active subspace is apparent in this plot, since more variation in P_{\max} is visible along the first active variable (the x -axis) than the second (the y -axis).

Lastly, Figures 3a and 3b show all 10000 evaluations of P_{\max} projected with the one- and two-dimensional active subspaces, where $\hat{\mathbf{w}}_1$ and $\hat{\mathbf{w}}_2$ are computed from $\hat{\mathbf{C}}$ in (6) using all 10000 realizations of the gradient. The trends visible in Figures 2a and 2b are further supported by plotting all realizations.

To create these figures, we evaluated the model $(m+1)(M)(M') = 60000$ times, which took approximately five minutes on a MacBook Air. A more expensive model would permit fewer evaluations, and we would choose M and M' differently.

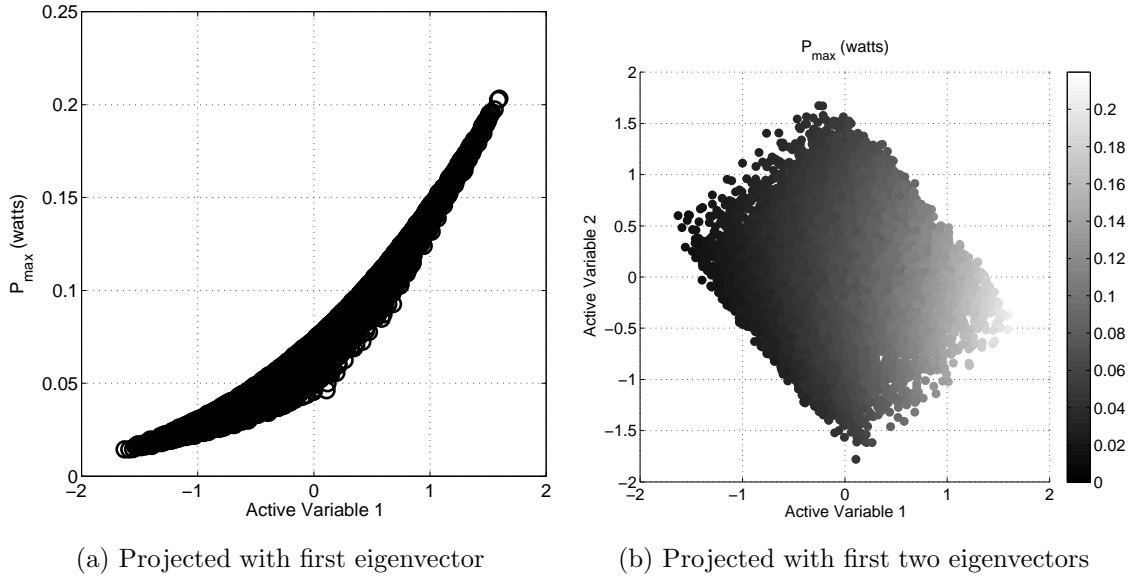


Figure 3: Visualizations of all realizations of P_{\max} with the inputs projected using the one-dimensional and two-dimensional active subspaces. The trend present in 2a and 2b is further supported by viewing all realizations.

5 Discussion and conclusions

The estimated eigenvalues in Table 2 and the plots in Figures 2 and 3 in Section 4 provide strong evidence for the presence of a dominant one-dimensional active subspace in the P_{\max} performance parameter computed from the single-diode model as a function of the model’s five input parameters. The natural question is how one can exploit the dimension reduction afforded by this apparent active subspace. There are five types of studies where one must explore the space of inputs that benefit greatly from fewer input parameters. To keep the scope of this paper limited, we do not address the details of any of these studies, and we prefer to reserve them for future exploration.

Visualization. The active subspace enables one to view the model output’s dependence on its inputs with standard computer graphics tools when the active subspace is not more than two-dimensional. Visualizations like those in Figures 2 and 3 can provide insights to modelers seeking to improve their models.

Optimization. Suppose one wanted to maximize P_{\max} over the input variables. The plot

in Figure 3 shows a monotonic trend in the univariate function of the first active variable. For such functions, maximization is trivial; simply make the first active variable $\mathbf{w}_1^T \mathbf{x}$ as large as possible subject to the constraints $\mathbf{x} \in [-1, 1]^m$. In general, a five-dimensional global optimization where the input/output relationship is not well understood is a difficult problem. For the P_{\max} output from the single-diode model, the active subspace provides a way to discover the location of the global optimum with ease.

Response surfaces. If the single-diode model were expensive to evaluate, then one may wish to construct a response surface that approximates the map from inputs to outputs. A one-dimensional active subspace allows one to build a response surface on only the active variable instead of the five model input parameters. Constructing a response surface in one variable is certainly preferred to constructing one in five variables. In addition, the visualization tools give one confidence that the response is sufficiently smooth with respect to the active variable to permit an accurate response surface.

Averages. If the input parameters are treated as random variables, then one may wish to compute an average of P_{\max} over all five input variables to get its expected value. Since the average of P_{\max} over its inputs is the same as the average of the conditional expectation given the active variable, we need only to approximate a marginal density of the active variable to compute the average. We are still working on the specifics of this idea, but the goal would be to transform a five-dimensional integral into a one-dimensional integral requiring many fewer evaluations of P_{\max} .

Calibration. Suppose a modeler wanted to design a solar cell with P_{\max} in a specified range and needed appropriate values for the model inputs. A one-dimensional active subspace makes this query much easier—especially if P_{\max} is monotonic with respect to the active variable as in Figure 3.

We have discussed methods for discovering a low-dimensional linear subspace that describes the variability in a model’s predictions with fewer parameters than the model’s natural inputs. We have applied this procedure to a single-diode solar cell model with key performance parameter P_{\max} , and we discovered a dominant one-dimensional active subspace. We offered several possible ways to exploit the knowledge of this low-dimensional parametric dependence to gain greater insight into the model.

References

- [1] Constantine, P. G., Wang, Q., Doostan, A., and Iaccarino, G. (2011). *A surrogate accelerated Bayesian inverse analysis of the HyShot II flight data*. American Institute of Aeronautics and Astronautics.
- [2] Constantine, P. G., Dow, E., and Wang, Q. (2014). Active subspace methods in theory and practice: applications to kriging surfaces. *SIAM Journal of Scientific Computing*. In press.
- [3] Cook, R. D. (2009). *Regression Graphics: Ideas for Studying Regressions Through Graphics*, volume 482. John Wiley & Sons.
- [4] De Soto, W., Klein, S. A., and Beckman, W. A. (2006). Improvement and validation of a model for photovoltaic array performance. *Solar Energy*, **80**, 78–88.
- [5] Farivar, G. and Asaei, B. (2010). Photovoltaic module single diode model parameters extraction based on manufacturer data sheet parameters. *Power and Energy (PECon)*, pages 929–934.
- [6] Hansen, C., Luketa-Hanlin, A., and Stein, J. (2013a). Estimation of parameters for single diode models using measured IV curves. *39th IEEE Photovoltaics Specialists Conference*.
- [7] Hansen, C., Luketa-Hanlin, A., and Stein, J. (2013b). Sensitivity of single diode models for photovoltaic modules to method used for parameter estimation. *28th European Photovoltaic Solar Energy Conference and Exhibition*, pages 3258 – 3264.
- [8] Jain, A. and Kapoor, A. (2004). Exact analytical solutions of the parameters of real solar cells using Lambert W-function. *Solar Energy Materials & Solar Cells*, **81**, 269–277.
- [9] Lukaczyk, T. W., Constantine, P. G., Palacios, F., and Alonso, J. J. (2014). *Active subspaces for shape optimization*. American Institute of Aeronautics and Astronautics.
- [10] Russi, T. M. (2010). *Uncertainty quantification with experimental data and complex system models*. Ph.D. thesis, UC Berkeley.

- [11] Saltelli, A., Ratto, M., Andres, T., Campolongo, F., Cariboni, J., Gatelli, D., Saisana, M., and Tarantola, S. (2008). *Global Sensitivity Analysis: The Primer*. John Wiley & Sons.
- [12] Samarov, A. M. (1993). Exploring regression structure using nonparametric functional estimation. *Journal of the American Statistical Association*, **88**(423), 836–847.
- [13] Wang, Q., Chen, H., Hu, R., and Constantine, P. G. (2011). *Conditional sampling and experiment design for quantifying manufacturing error of transonic airfoil*. American Institute of Aeronautics and Astronautics.
- [14] Zaharatos, B., Campanelli, M., Hansen, C., Emery, K., and Tenorio, L. (2014). Likelihood methods for single-diode model parameter estimation from noisy I-V curve data. *40th IEEE Photovoltaics Specialists Conference*.